Leukocyte Complexity Predicts Breast Cancer Survival and Functionally Regulates Response to Chemotherapy

SUPPLEMENTAL MATERIALS AND METHODS

SUPPLEMENTAL FIGURES

SUPPLEMENTAL REFERENCES

David G. DeNardo[1,#], Donal J. Brennan[2], Elton Rexhepaj[2], Brian Ruffell[1], Stephen L. Shiao[3], Stephen F Madden[4], William M. Gallagher[2], Nikhil Wadhwani[1], Scott D. Keil[1], Sharfaa A. Junaid[1], Hope S. Rugo[5,6], E. Shelley Hwang[6,7], Karin Jirström[8], Brian L. West[9], Lisa M. Coussens[1,6,*]

SUPPLEMENTAL MATERIALS AND METHODS:

TMA Immunohistochemistry: Tissue microarray slide sections (4.0 μm) were deparaffinized in xylene, and re-hydrated through descending concentrations of ethanol. For CD4 and CD8 detection, heat-mediated antigen retrieval was performed using microwave treatment for 7 min in a citrate buffer (BioGenex) followed by 3 serial 5 minute washes in phosphate buffered saline (PBS). Antigen retrieval for CD68 detection was accomplished by treatment of slides with Protinase XXV (Lab Vision Inc.) for 5 minutes followed by 4 serial 5 minute washes in PBS. Endogenous peroxidase activity was blocked by incubating slides in 5% hydrogen peroxide (Sigma) diluted in methanol for 20 min, followed by 4 serial washes in PBS. To reduce nonspecific background, slides were pretreated with blocking buffer (10% goat serum [Invitrogen], 1.0 % bovine serum albumen (Sigma) dissolved in PBS) for 30 min. Primary antibodies were pre-diluted in blocking buffer to 1:100 for CD68 (KP-1, NeoMarkers) and CD8 (C8/144B, NeoMarkers) or 1:25 for CD4 (368, Novocastra) and applied to tissue section for 16 hours at 4°C. Signal amplification and development were accomplished utilizing the Ultravision LP Detection System (Thermo Scientific) according to manufactures guidelines. For additional markers IHC analysis was performed in the Ventana Benchmark system (Ventana Medical Systems Inc, AZ) using pre-diluted antibodies to ER (Anti-ER, clone 6F11), PR (Anti-PgR, clone 16) and Her2 (Pathway CB-USA, 760-2694) or in the Dako Techmate 500 system (Dako, Glostrup, Denmark) for Ki-67 (1:200, M7240; Dako).

Human BC Subtyping: Molecular sub-typing was performed using IHC as previously described by Carey *et al* (1). Tumors were classified as Luminal A (ER^+, PR^+, $HER2^-$), Luminal B (ER^+, PR^+, $HER2^+$), HER2 (ER^-, PR^-, $HER2^+$), or triple negative (ER^-, PR^-, $HER2^-$).

Biochemical selectivity and potency of PLX3397: PLX3397 selectively inhibits the c-Fms and the c-Kit receptor tyrosine kinases, with biochemical IC_{50} values of 0.02 μM and 0.01 μM respectively (**Figure S6A**). PLX3397 was identified as a potent CSF-1R and c-KIT kinase inhibitor by using a Scaffold- and X-ray structure-based discovery approach (2-4). In a comprehensive screen of 226 different kinases, including representatives of all protein kinase subfamilies and several lipid kinases (Invitrogen SelectScreen™ profiling service), PLX3397 at 0.03 μM and 1.0 μM only inhibited five other kinases significantly. PLX3397 was selected based on inhibition of the CSF1-dependent proliferation of the murine myelogenous leukemia cell line M-NFS-60, with an IC_{50} of 0.44 μM the murine macrophage cell line Bac1.2F5, with an IC_{50} of 0.22 μM. The human acute megakaryoblastic leukemia cell line M-07e, which depends on the addition of SCF for growth, was inhibited by PLX3397 with an IC_{50} of 0.1 μM. These sub-micromolar potencies confirm that PLX3397 can enter cells and inhibit Fms-driven cell growth.

Immunohistochemistry and Image Analysis: Murine tissues: Paraffin-embedded tissue sections were fixed in 10% formalin and incubated with detection antibodies as previously described (5). A biotinylated secondary antibody was applied, followed by incubation with streptavidin-conjugated HRP. Peroxidase activity was localized with diaminobenzidine (Vectastain ABC kit, Vector Laboratories). To determine proliferation index mice received intraperitoneal injections of bromodeoxyuridine (BrdU; Roche Diagnostics) dissolved in PBS (50 μg per g of mouse body weight) 90 min prior to sacrifice. 5.0-mm thick paraffin sections were deparaffinized in xylene, rehydrated in graded ethanol, and subjected to antigen retrieval by steam heating in CitraTM antigen retrieval solution (BioGenex). BrdU-positive cells were detected according to manufacturers recommendations using the anti-BrdU antibodies (MCA2060, Serotec). To detect endothelial cells and apoptotic cells, endothelium specific marker PECAM1/CD31 and cleaved caspase 3 were visualized on paraffin-embedded tissue sections. For antigen retrieval, tissue sections were subjected to steam heating in CitraTM antigen retrieval solution (BioGenex). Non-specific binding was blocked using PBS containing 5% goat serum (Thermo Fisher) and 2.5% BSA (Blocking buffer). Sections were incubated with rat anti-mouse CD31 (1:50, BD Biosciences) and rat anti-mouse cleaved caspase 3, (1:100, Cell Signaling) in 0.5X blocking buffer for 2 hr at room temperature. Sections were then incubated with biotinylated rabbit anti-rat IgG secondary antibodies (1:200, Vector Laboratories) for 45 min at room temperature. Slides were subsequently incubated with horseradish peroxidase conjugated avidin complex (ABC Elite, Vector Laboratories) for 30 min, followed by incubation with Fast 3,3 diaminobenzidine (DAB, Vector Laboratories). Sections were counterstained with methyl green, dehydrated, and mounted with Cytoseal 60 (Thermo Fisher).

Analysis of $F480^+$ $CD4^+$ and $CD8^+$ cells was performed by IHC on 10-μm thick frozen sections. Antigen retieval was conducted using ice-cold methanol for 5 minutes. Slides were blocked with goat sera and primary antibodies against F480 (1:100, Serotec), CD31 (1:50, BD Pharmingen), CD4 (1:100, BD Pharmingen) and CD8 (1:100, BD Pharmingen). For immunofluorescent staining Alexa fluor 594 and 488 conjugated goat anti-rat (Molecular Probes, 10 mg/ml) or alternatively strepavidin conjugated 594 were used. All immuno-localization experiments were repeated on multiple tissue sections and included negative controls for determination of background staining, which was negligible. All colorimetric stains were exposed as described above.

Murine Tissue Image Analysis

Fully automated image acquisition was employed using he Aperio ScanScope CS Slide Scanner (Aperio Technologies) system with a 20x objective to capture whole-slide digital images and the positive pixel count algorithm (Aperio Technologies) was employed to develop a qualitative scoring model. Briefly, CD31+ vessels

were quantitated from invasive carcinoma tissue using the Aperio default-vessel algorithm, while BRDU and Cleaved Caspase used the nuclear-9 algorithm (Aperio) to assess entire tumor tissue.

Quantitative RT-PCR: Total tissue RNA was extracted from snap frozen tumor tissue or lysed tissue culture cells using an RNeasy Mini Kit (QIAGEN). cDNAs were synthesized using Superscript III first-strand synthesis (Invitrogen). Primers specific for *β-actin, GAPDH, 18s VEGF, MCP1, MCP2, MCP3, IL2, IL12p35, IFNγ, IFNα1 IFNαβ1, ARG1 and IL34* (Superarray) were used and relative gene expression was determined using RT_2 Real-Time SYBR Green/ROX PCR master mix (Superarray) on an ABI 7900HT quantitative PCR machine (ABI biosystems). The comparative threshold cycle method was used to calculate fold change in gene expression, which was normalized to *β-actin* and *GAPDH and/*or *18S* as reference genes.

Flow cytometry analysis: Single-cell suspensions were prepared from mammary gland dissection by manual mincing using scalpel followed by enzymatic digestion for 40 min at 37°C by collagenase A 3.0 mg/ml (Roche) and DNase I (Roche) dissolved in DMEM (Invitrogen), under stirring conditions. Digestion mixtures were quenched by adding DMEM containing 10% FBS and then filtered through 0.7 μm nylon strainers (Falcon). Cells were then incubated for 10 min at 4°C with rat anti-mouse CD16/CD32 mAb (BD Biosciences) at a 1:100 dilution in PBS containing 1.0% of BSA (Sigma) to prevent nonspecific antibody binding. Subsequently, cells were washed twice in PBS/BSA and incubated for 20 min with 100 μl of fluorophore-conjugated anti-mouse antibodies; B220 (RA3-6B2), CD3e (145-2C11), CD4 (6K1.5), CD8a (53-6.7), CD11b (M1/70), CD11c (N418), CD14 (Sa2-8), CD19 (MB19-1), Ly6C (HK1.4), Ly6G (1A8), CD44 (IM7), CD45 (30-F11), CD80 (16-10A1), CD86 (GL1), CD115 (AFS98), F4/80 (BM8) and/or MHCII (M5/114.15.2) (all from eBioscience) followed by two washes with PBS/BSA. 7-AAD (BD Biosciences) was added (1:10) to discriminate between viable and dead cells; alternatively live/dead aqua was used (Invitrogen). For human primary tumor samples, single cell suspensions were prepared as described above. Cells were then incubated for 10 min at 4°C with rat anti-human CD16/CD32 mAb (BD Biosciences) at a 1:100 dilution and then washed twice. Cells were stained with 100 μl of fluorophore-conjugated anti-human antibodies; CD45(HI30) and CD14 (61D3) (Invitrogen) and CD3e (OKT3), CD8a (53-6.7) and CD11b (M1/70), (all from eBioscience) followed by two washes with PBS/BSA. Data acquisition and analysis for both human and mouse were performed on a FACSCalibur using CellQuestPro software (BD Biosciences) or LSRII (BD Biosciences) using the FlowJo version 8.8 software (Tree Star).

Immune cell isolation: Immune cells were isolated from tumors using a dual purification strategy including magnetic purification followed by flow sorting. Single cell suspensions from tumors were created as described

above. Cells were then incubated for 10 min at 4°C with rat anti-mouse CD16/CD32 mAb (BD Biosciences) at a 1:100 dilution in PBS/BSA then washed twice in PBS/BSA and incubated for 20 min with appropriate fluorescent primary antibodies which included anti-CD45-APC (30-F11), in addition to anti-CD4 (GK1.1), -CD3 (145-2C11), -Gr-1 (RB6-8G5), -CD11b (93) and/or F4/80 (BM8) (all from eBiosciences) at 1:100 dilution depending on the population to be isolated. Total leukocytes were isolated using magnetic bead selection for APC_+ according to manufactures specifications (Miltenyi Biotec). Magnetically selected cells were then flow sorted on a FACSAria using CellQuestPro software (BD Biosciences).

TAM repression assay: TAMs were isolated from late stage tumors from 100-day-old MMTV-PyMT mice. Tumors were disaggregated and stained for CD45 as described above. Single cell suspensions were passed through 0.7 μm nylon strainers (Falcon). Cells were then incubated for 10 min at 4°C with rat antimouse CD16/CD32 mAb (BD Biosciences) at a 1:100 dilution in PBS/BSA then washed twice in PBS/BSA and incubated for 20 min with appropriate fluorescent primary antibodies which included anti-CD45-APC (30-F11), in addition to anti-Gr-1 (RB6-8G5), -CD11b (93) and/or F4/80 (BM8) (all from eBiosciences) at 1:100 dilution depending on the population to be isolated. Total leukocytes were isolated using magnetic bead selection for APC_+ according to manufactures specifications (Miltenyi Biotec). Magnetically selected cells were then flow sorted on a FACSAria using CellQuestPro software (BD Biosciences). T cells were purified using the CD8+ T cell isolation kit from Miltenyi Biotec via negative selection. The resulting purified T cell suspension was labeled with CFSE (Invitrogen). $1x10^5$ CFSE labeled $CD8^+$ T cells and selected TAMs were concomitantly added to CD3/CD28 coated plates (1.0 μg/ml each, eBioscience) to induce T cell proliferation. Analysis of cells was performed on a LSRII after labeling with fluorescent antibodies and 7AAD (BD Bioscience) to exclude dead cells (as described above).

Leukocyte chemotaxis assay: For cell migration, PBLs were collected from peripheral blood of FVB/n mice following cardiac puncture, and seeded (10^5 cells/ 100 μl DMEM containing 0.1% BSA) onto the top chamber of transwell filters (3-μm; Corning). Filters were placed in a 24-well plate that contains conditioned medium isolated from vehicle or PTX (20 nM) pretreated MMTV-PyMT-derived MECs. For some conditions, PLX3397 (50 nM) was added to the upper chamber. 6-hr following incubation, the media in the lower chamber was isolated and analyzed by flow cytometry for CD11b, CD3 and 7AAD as described above. Samples were run in triplicates for each experimental group and experiments were repeated twice.

Retrospective gene expression survival analysis: Gene expression data sets were downloaded from the Gene Expression Omnibus (http://www.ncbi.nlm.nih.gov/geo/) or authors' websites in the form of raw data files

where possible. Only datasets with clinical survival information and at least 50 patients were included. Table S8 provides a list of the datasets used. In total 3,872 samples across 14 different platforms were analyzed. Were raw data was not available, the normalized data as published by the original study was used. In the case of the affymetrix datasets (.cel files), gene expression values were called using the robust multichip average method(6) and data were quantile normalized using the Bioconductor package, affy (www.bioconductor.org). For the dual-channel platforms, data were loess normalized (7) using the Bioconductor package limma. Hybridization probes were mapped to Entrez gene IDs (8). The Entrez gene IDs corresponding to the array probes were obtained using Biomart (www.biomart.org/) and the Bioconductor annotation libraries. Probes that hit multiple genes were filtered out. If there were multiple probes for the same gene, the probes were averaged for that gene. All calculations were carried out in the R statistical environment (http://cran.r-project.org/).

Relapse-free survival (RFS) of untreated patients was considered the survival end point. When RFS was not available, distant metastasis–free survival (DMFS) data was used and if neither RFS nor DMFS were available overall survival (OS) was used. Median expression for both CD8 and CD68 was used to determine high and low groups within each of the 22 individual datasets. Once a sample was assigned to a particular group the 22 datasets were combined and a global survival analysis was performed. It is important to treat each dataset separately when determining if a sample belongs to the high or low expression groups, as the expression of the CD8 and CD68 will vary greatly across the different experiments/platforms. The survival curve was based on Kaplan-Meier estimates. The R package survival was used to calculate and plot the Kaplan-Meier survival curve.

SUPPLEMENTAL FIGURES AND LEGENDS:

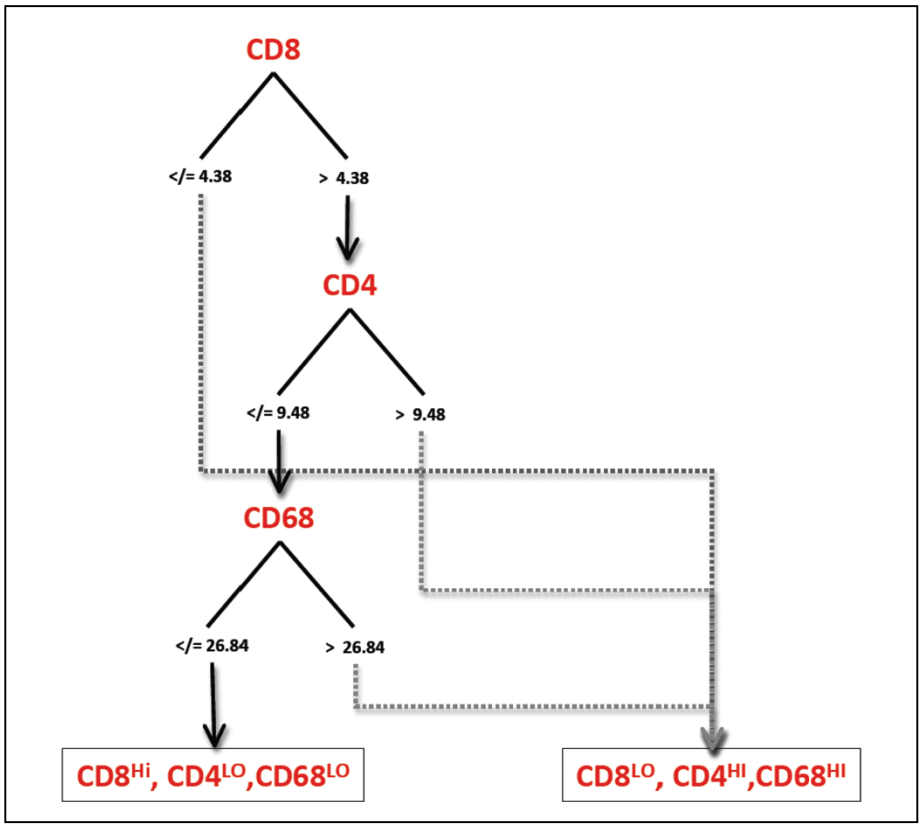

Figure S1. Development of the CD68/CD4/CD8 signature.

Regression tree analysis used to define the signature based on continuous immune cell density data. All cases were defined as $CD68^{high}/CD4^{high}/CD8^{low}$ and $CD68^{low}/CD4^{low}/CD8^{high}$ as demonstrated. The signature was defined in Cohort I, and validated using the same thresholds in Cohort II.

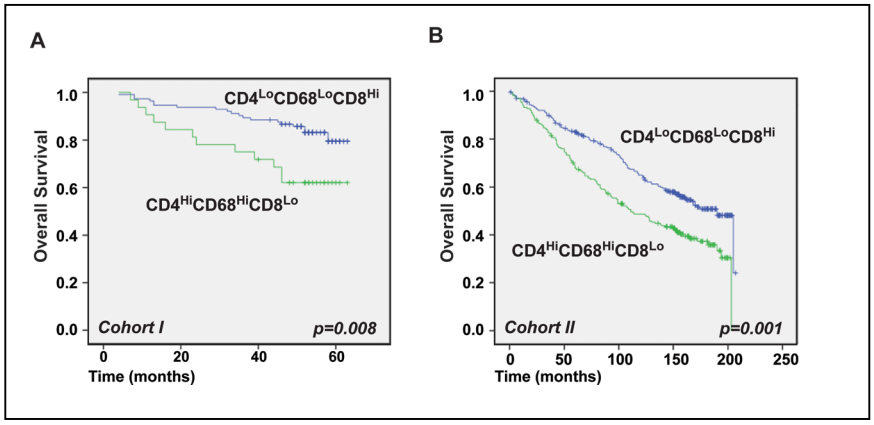

Figure S2. CD68/CD4/CD8 immune-profile signature is an independent prognostic indicator of overall survival in breast cancer patients.

A-B) Kaplan-Meier estimate of overall survival (OS) comparing $CD68^{high}/CD4^{high}/CD8^{low}$ and $CD68^{low}/CD4^{low}/CD8^{high}$ immune profiles as assigned by random forest clustering employed to identify optimum thresholds using Cohort I (**C**). Identified $CD68^{high}/CD4^{high}/CD8^{low}$ and $CD68^{low}/CD4^{low}/CD8^{high}$ immune profiles were employed to stratify a second independent cohort, Cohort II (**D**). Cohort I (n=179) and Cohort II (n=498) samples were assessed and the log rank (Mantel-Cox) p value is denoted for difference in OS.

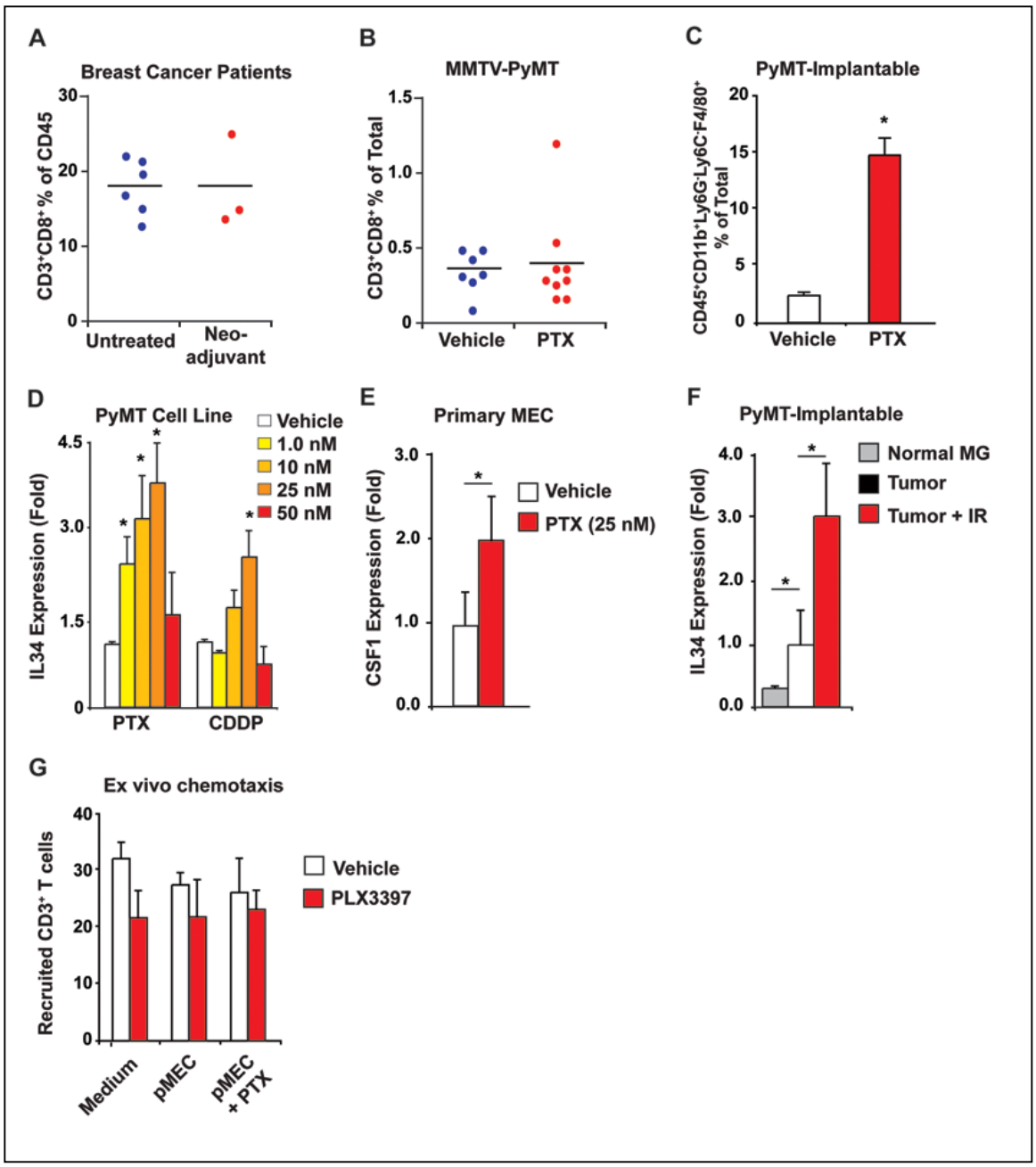

Figure S3: Cytotoxic Therapy Induces CSF1-Dependent Macrophage Recruitment.

A) Percentage of $CD8^+$ CTLs from fresh human BC samples depicted as mean number of $CD45^+CD3^+CD8^+$ T lymphocytes as a % of total $CD45^+$ cells +/- SEM (analyzed by flow cytometry). "Neo-adjuvant" denotes patients who received chemotherapy prior to surgical resection of their primary BC as opposed to those who did not, denoted as "Untreated".

B) $CD8^+$ CTL percentage in MMTV-PyMT mice following PTX treatment. Data are depicted as mean number of $CD45^+CD3^+CD8^+$ T lymphocytes as a % of total cells +/- SEM (analyzed by flow cytometry, >5 mice/group).

C) FACS analysis of TAM percentage in orthotopic PyMT-derived tumors following PTX. Implanted tumors were allowed to grow to a median diameter of 1.0 cm when mice received PTX for 15 days and total number of $CD45^+Ly6G^-Ly6C^-CD11b^+F4/80^+$ TAMs depicted as mean % of total cells +/- SEM (4 mice/group).

D-E) Dose-dependent expression of IL-34 mRNA following chemotherapy. QRT-PCR analysis of mRNA expression in pMECS isolated from MMTV-PyMT (**D) or** MECs isolated from nontransgenic female FVB/n mice (**E**) 24 hours after treatment with either cisplatin (CDDP) or PTX expressed as mean fold change compared to vehicle treated cells +/- SEM. Chemotherapy doses are shown. Samples were assayed in triplicate for each condition.

F) Expression of IL-34 following ionizing radiation. QRTPCR analysis of mRNA expression from orthotopically-implanted PyMT tumors 2 days after treatment with ionizing radiation (10 Gray) expressed as mean fold changeas compared to control (sham-treated) animals.

In all panels (*) denotes statistically significant differences ($p<0.05$ by Mann-Whitney).

G) $CD45^+CD3^+$ cell migration in response to conditioned medium from MMTV-PyMT-derived MECs (pMECs) treated with PTX (25 nM for 24 hours) as compared to vehicle control, evaluated by Boyden chamber assay. $CD45^+CD3^+$ PBLs migrating to the lower chamber in the presence and absence of 10 nM PLX3397 visualized by flow cytometry. Data are depicted as mean cell number assayed in triplicate for each tested condition.

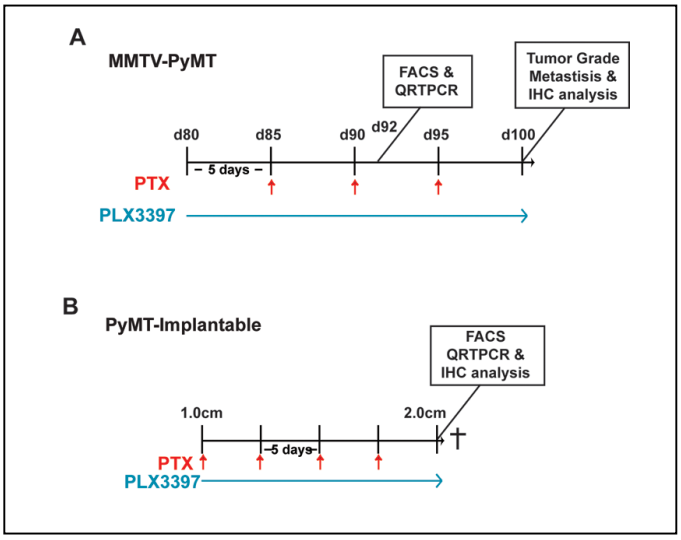

Figure S4: Treatment Regimens and Analysis.

A-B) Schematic depicts treatment regimens and schedule for tissue collection for **A**) MMTV-PyMT mice and **B**) orthotopic PyMT-tumor bearing mice

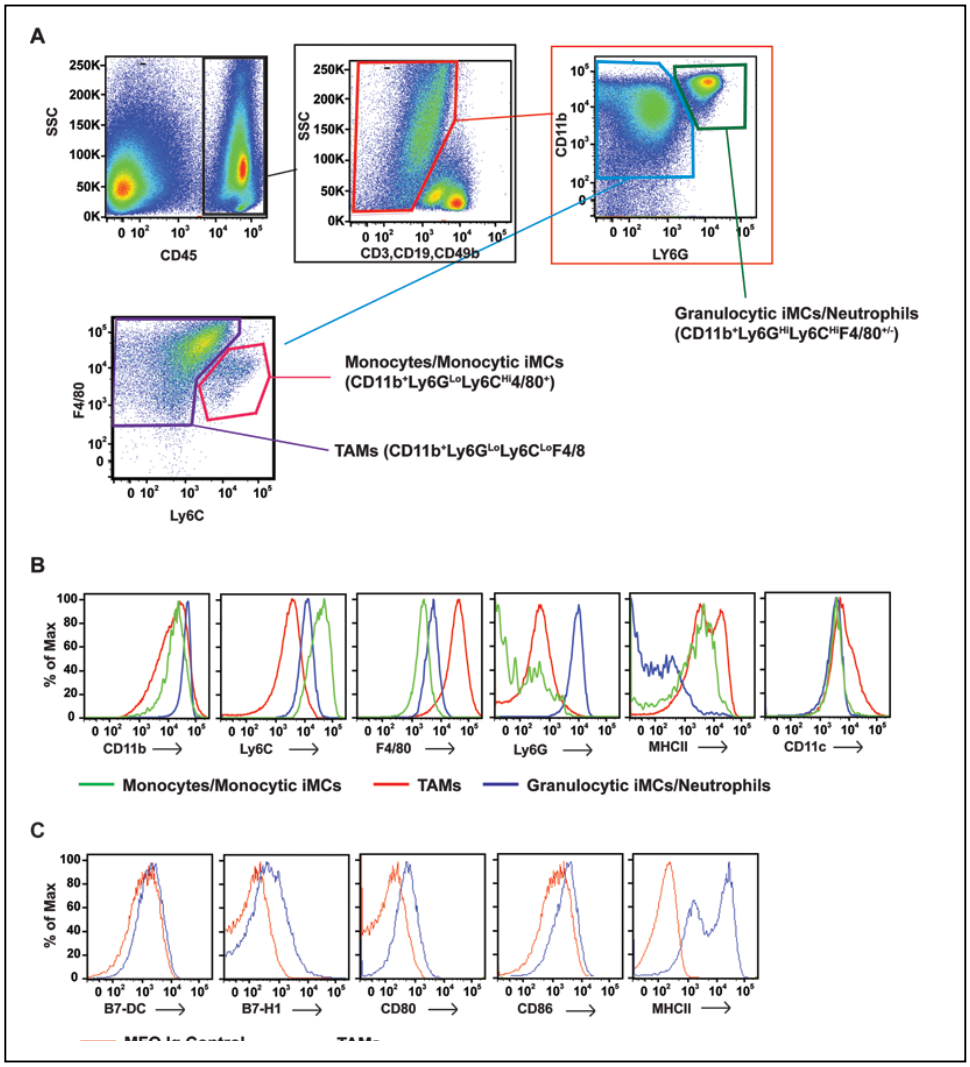

Figure S5: Analysis of Immune Infiltrate.

A) Representative flow cytometry of tumors from 92-day-old MMTV-PyMT mice depicting gating strategy used for analysis of TAMs, iMCs and monocytes.

B) Representative MFI plots depicting expression of maturation and differentiation markers for TAMs, monocytes and granulocytic iMCs.

C) Representative MFI plots depicting TAM expression of B7H1, B7DC, MHCII, CD80 and CD86 in mammary tumors of 95 day-old MMTV-PyMT mice.

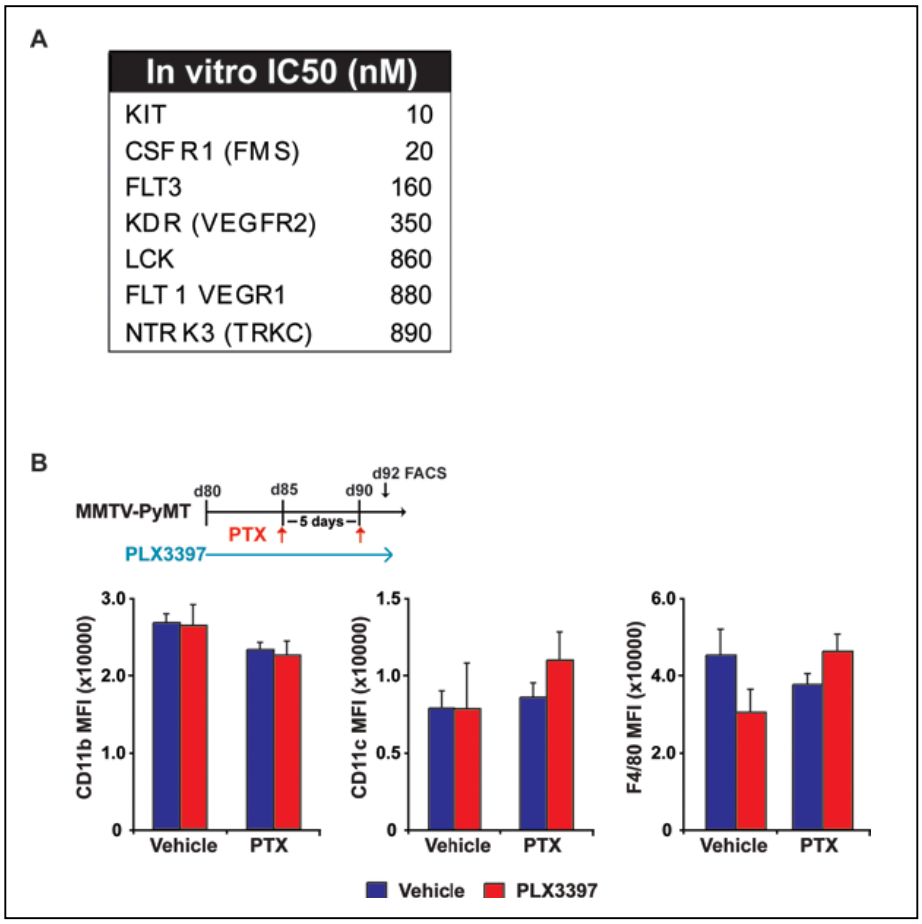

Figure S6: Cell responses to PTX/PLX3397 therapy

A) IC_{50} in nM for kinases inhibited by PLX3397 *in vitro*. PLX3397 selectively inhibits the cFMS/CSF1R and the cKIT receptor tyrosine kinases, with biochemical IC_{50} values of 0.02 µM and 0.01 µM respectively. In a comprehensive screen of 226 different kinases, including representatives of all protein kinase subfamilies and several lipid kinases (Invitrogen SelectScreen™ profiling service), PLX3397 at 0.03 µM and 1.0 µM only inhibited five other kinases significantly. These kinases were confirmed to have biochemical IC_{50} values at least 8-fold higher then Fms/CSF1R or Kit.

B) Neither PLX3397 nor PTX alters TAM differentiation. Expression of differentiation markers F4/80, CD11b and CD11c are depicted for $CD45^{+}Ly6G^{-}Ly6C^{-}CD11b^{+}F4/80^{+}$ TAMs as mean MFI from MMTV-PyMT mice (>5/group) treated with vehicle, PTX and/or PLX3397. Treatment schematic is shown.

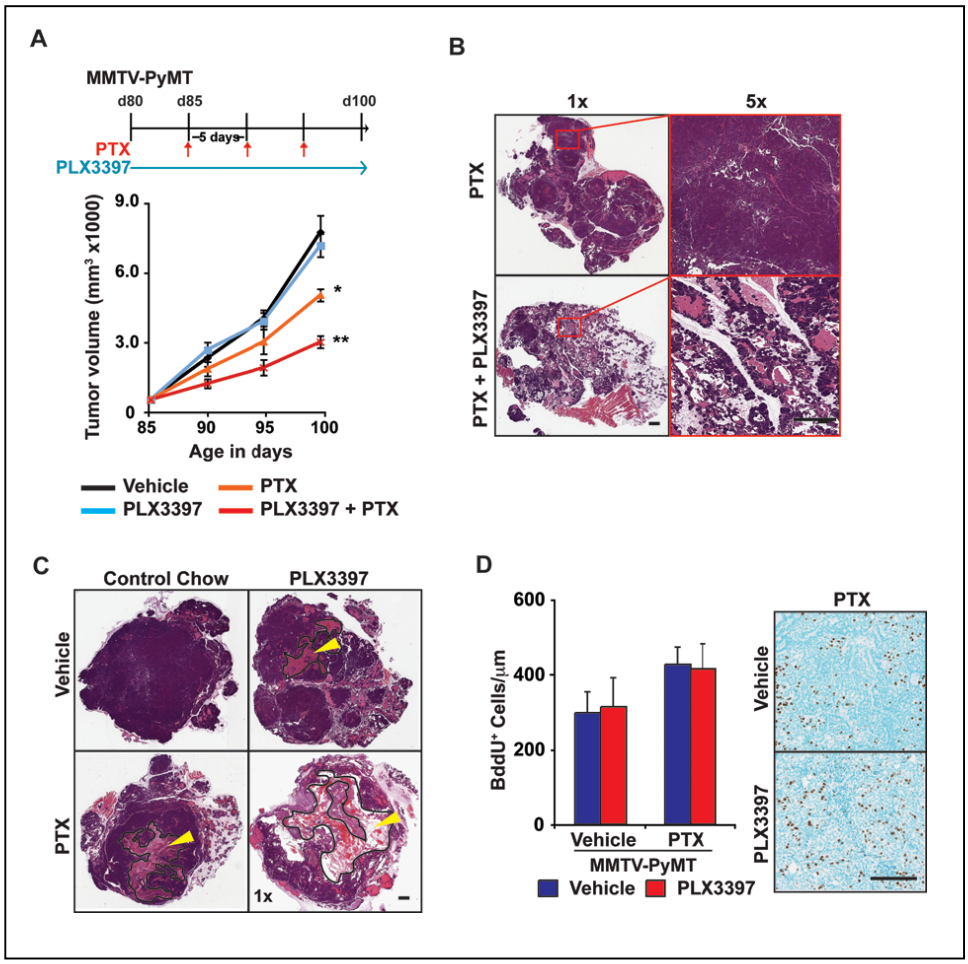

Figure S7: Combined PTX/PLX3397 treatment regulates characteristics of mammary tumors.

A) Treatment with PTX in combination with PLX3397 slows tumor development. 85-day-old MMTV-PyMT mice were treated with PTX +/- PLX3397, and total tumor burden/animal assessed every 5 days until endpoint. Treatment regimen is depicted and data are displayed as mean tumor burden +/-SEM. (*) Indicates statistically significant differences between vehicle versus PTX-treated mice, while (**) indicates significant differences between PTX alone versus PTX/PLX3397 treated mice.

B) Representative photomicrographs of whole mammary glands removed from 100-day-old MMTV-PyMT mice treated with PTX with or without PLX3397. Scale bar = 500 μm.

C) Representative photomicrographs of late-stage carcinomas from 100-day-old MMTV-PyMT mice treated with vehicle or PTX and/or PLX3397. Arrowheads (yellow) indicate necrotic areas. Scale bar = 500 μm.

D) Quantitation of BrdU-positive MECs in mammary tumors of MMTV-PyMT mice treated PTX and/or PLX3397 versus vehicle controls. Graph shows mean positive cells per μm of tumor. Representative photomicrographs show BrdU-positive cells (brown staining) in mammary tumors of MMTV-PyMT mice. Scale bar = 500 μm.

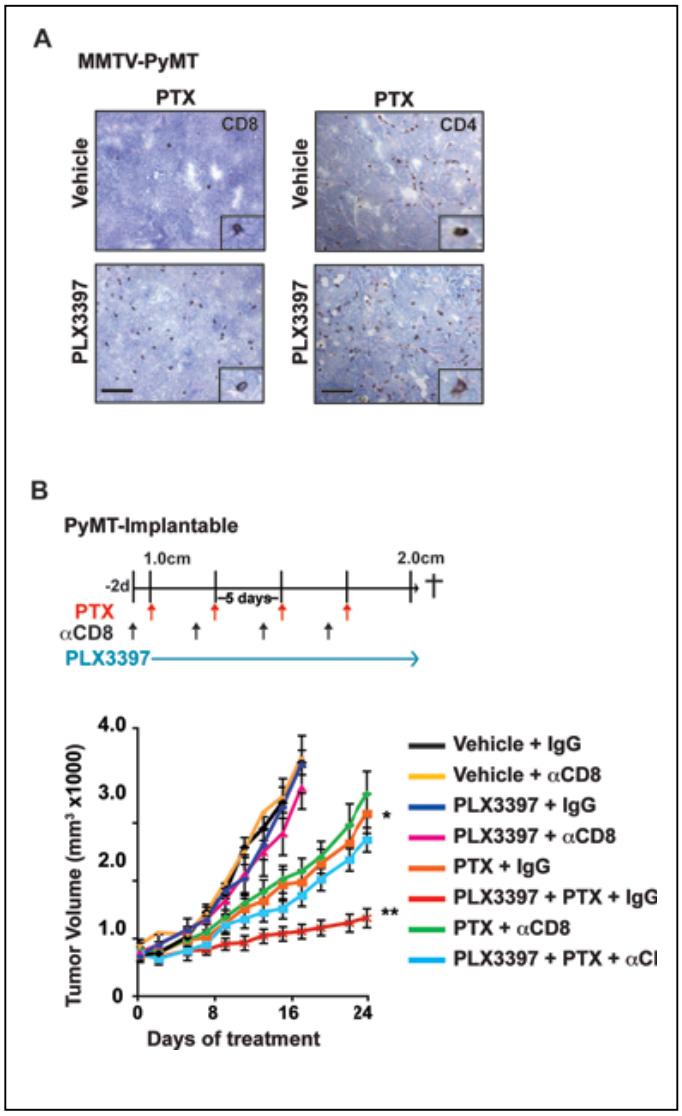

Figure S8: Combined PLX3397 and PTX induce anti-tumor T cell responses *in vivo*.

A) Combined PTX/PLX3397 enhances tumor infiltration of T lymphocytes. Immunodetection of tumor infiltrating $CD8^+$ and $CD4^+$ T lymphocytes in tumor tissue from MMTV-PyMT mice treated with either PTX alone, or in combination with PLX3397. Representative photomicrographs show tumor-infiltrating T cells (brown staining). Scale bar = 100 μm.

B) Improved outcome of PLX3397/PTX-treated mice is $CD8^+$ T cell-dependent. Orthotopic-implanted PyMT-derived tumors were grown to a median diameter of 1.0 cm when mice were then treated with PTX and/or PLX3397, in combination with anti-CD8 or control IgG for 21 days, and tumor burden/animal assessed every 2-3 days. Treatment regimens are depicted. Some data are the same as **Figure 6B** but contain additional treatment groups. (*) Indicates statistically significant differences between PTX alone and PTX/PLX3397 treated mice; (**) indicates significant differences between PTX/PLX3397 treated mice treated with anti-CD8 and PTX/PLX3397.

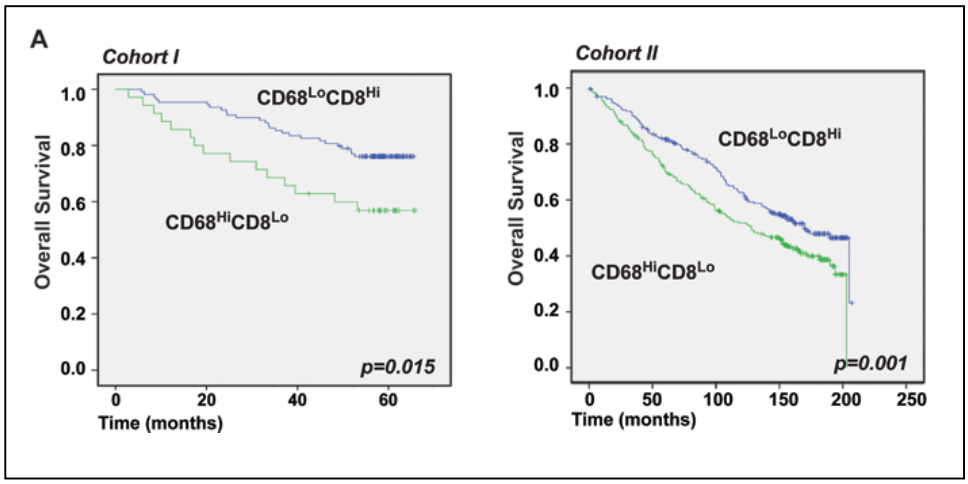

Figure S9. CD68/ CD8 immune-profile signature is an independent prognostic indicator of overall survival in breast cancer patients.

Kaplan-Meier estimate of overall survival (OS) comparing $CD68^{high}/CD4^{high}/CD8^{low}$ and $CD68^{low}/CD4^{low}/CD8^{high}$ immune profiles as assigned by random forest clustering employed to identify optimum thresholds using Cohort I. Identified $CD68^{high}/CD8^{low}$ and $CD68^{low}/CD8^{high}$ immune profiles were employed to stratify Cohort II. Cohort I (n=179) and Cohort II (n=498) samples were assessed and the log rank (Mantel-Cox) p value is denoted for difference in OS.

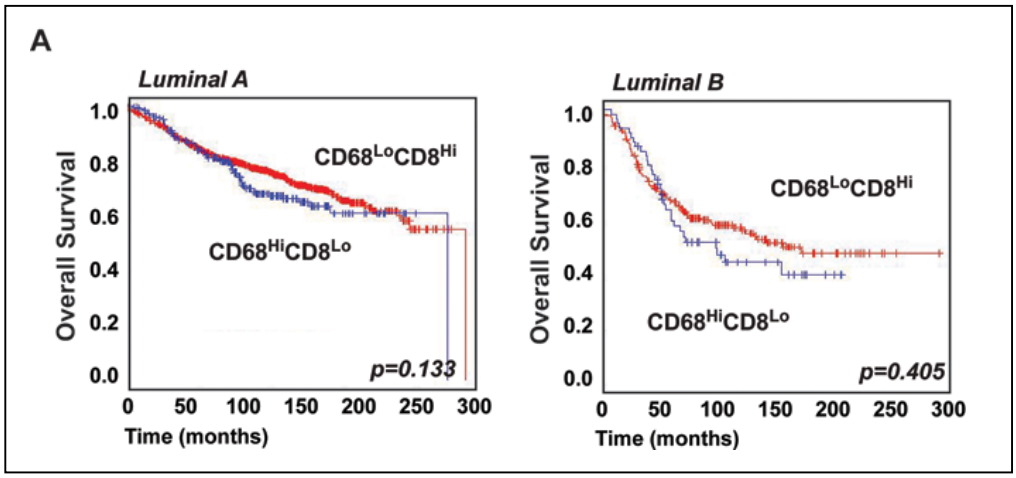

Figure S10: Ratio of CD68 to CD8 does not predict patient survival in Luminal BCs.

Kaplan-Meier estimate of overall survival comparing $CD68^{high}/CD8^{low}$ and $CD68^{low}/CD8^{high}$ mRNA expression from 3,872 patient samples across 14 different platforms. Median expression for both *CD8* and *CD68* was used to determine high and low groups within each of the 22 individual datasets. Once a sample was assigned to a particular group, the 22 datasets were combined and a global survival analysis was performed. Patient samples for tumors stratified into Luminal A and Luminal B BC and Kaplan-Meier estimates are depicted. The log rank (Mantel-Cox) p-value is denoted for difference in survival.

SUPPLEMENTAL TABLES

Table S1: Spearman Rho analysis for correlation between stromal CD68 and CD8 counts

Spearman Rho Correlation		CD8 Stromal Count	CD68 Stromal Count
Stromal CD8 Count	Correlation Coefficient	1.000	-0.382*
	Significance (2-tailed)	-	<0.001
Stromal CD68 Count	Correlation Coefficient	-0.382*	1.000
	Significance (2-tailed)	<0.001	-

*, indicates correlation with statistically significant p value

Table S2: Results from multivariate Cox regression analysis of overall survival (OS) for the CD68/CD4/CD8 signature in Cohort I

OS Cohort I	95% CI for HR			
	HR	Lower	Upper	P Value
Immune Signature	3.510	1.342	9.180	0.010
Grade	0.556	0.186	1.665	0.294
Nodal Status	2.461	0.939	6.449	0.067
Size	1.152	0.400	3.316	0.793
Ki67	8.388	1.693	41.561	0.009
Age	1.033	0.999	1.069	0.057
ER	0.535	0.137	2.090	0.368
PR	0.541	0.195	1.501	0.238
Her2	1.430	0.971	2.106	0.070

OS, overall survival; CI, confidence interval; HR, hazard ratio; ER, estrogen receptor; PR, progesterone receptor, Her2, Human epidermal growth factor receptor 2

Table S3: Results from multivariate Cox regression analysis of overall survival (OS) for the CD68/CD4/CD8 signature in Cohort II.

OS Cohort II	95% CI for HR			
	HR	Lower	Upper	P Value
Immune Signature	1.676	1.142	2.460	0.008
Grade	1.900	1.241	2.909	0.003
Nodal Status	2.394	1.627	3.524	<0.001
Size	1.006	0.997	1.014	0.178
Ki67	0.867	0.558	1.347	0.527
Age	1.047	1.029	1.065	<0.001
ER	0.836	0.483	1.446	0.522
PR	0.495	0.321	0.763	0.001
Her2	1.128	0.806	1.241	0.999

OS, overall survival; CI, confidence interval; HR, hazard ratio; ER, estrogen receptor; PR, progesterone receptor, Her2, Human epidermal growth factor receptor 2

Table S4: Multivariate Cox regression analysis of recurrence-free survival (RFS) for the CD68/CD4/CD8 signature in Cohort I

RFS Cohort I	95% CI for HR			
	HR	Lower	Upper	P Value
Immune Signature	2.788	1.002	7.772	0.050
Grade	1.266	0.412	3.888	0.681
Nodal Status	5.081	1.726	14.95	0.003
Size	1.038	1.016	1.060	0.001
Ki67	0.262	0.029	2.374	0.233
Age	1.033	0.997	1.070	0.072
ER	0.264	0.063	1.107	0.069
PR	1.349	0.389	4.676	0.637
Her2	6.170	2.015	18.89	0.001

OS, overall survival; CI, confidence interval; HR, hazard ratio; ER, estrogen receptor; PR, progesterone receptor, Her2, Human epidermal growth factor receptor 2

Table S5: Multivariate Cox regression analysis of recurrence-free survival (RFS) for the CD68/CD4/CD8 signature in Cohort II

RFS Cohort II	95% CI for HR			
	HR	Lower	Upper	P Value
Immune Signature	2.368	1.433	3.912	0.001
Grade	2.024	1.181	3.468	0.010
Nodal Status	2.724	1.643	4.514	<0.001
Size	0.998	0.998	1.009	0.748
Ki67	1.441	0.787	2.638	0.237
Age	0.998	0.980	1.015	0.784
ER	1.523	0.807	2.873	0.194
PR	0.327	0.188	0.570	<0.001
Her2	0.965	0.747	1.246	0.785

OS, overall survival; CI, confidence interval; HR, hazard ratio; ER, estrogen receptor; PR, progesterone receptor, Her2, Human epidermal growth factor receptor 2

Table S6: Multivariate Cox regression analysis of recurrence-free survival for the CD68/CD4/CD8 signature in lymph-node positive patients from Cohort II.

RFS Node+ Cohort II	95% CI for HR			
	HR	Lower	Upper	P Value
Immune Signature	1.858	1.008	3.423	0.047
Grade	1.150	0.600	2.205	0.673
Nodal Status	-	-	-	-
Size	1.647	0.907	2.990	0.101
Ki67	1.760	0.867	3.573	0.118
Age	0.759	0.377	1.529	0.440
ER	1.559	0.667	3.642	0.305
PR	0.429	0.236	0.780	0.006
Her2	1.487	0.730	3.029	0.274

OS, overall survival; CI, confidence intervat; HR, hazard ratio; ER, estrogen receptor; PR, progesterone receptor, Her2, Human epidermal growth factor receptor 2

Table S7: Patient cohort utilized for flow cytometry analysis of BC-infiltrating leukocytes

Age	Histology	Grade	ER	PR	Her2	Tumor Size	Node	Neoadjuvant Therapy
63	IDC	3	1+ (0)	1+ (1)	1+ (1.1)	1.6 cm	-	None
56	IDC	3	3+ (95)	3+ (90)	1+	2.6 cm	+	None
57	IDC	2	3+ (99)	3+ (25)	0	6.0 cm	+	None
61	IDC	3	3+ (95)	3+ (60)	2+ (1.1)	4.5 cm	+	None
78	IDC	3	3+ (40)	1+ (0)	3+	2.2 cm	+	None
54	ILC	2	3+ (30)	3+ (30)	1+	7.0 cm	+	None
73	IDC	2	3+ (100)	3+ (50)	3+	9.8 cm (4.2)	+ (+)	Paclitaxol, Cyclophosphamide, Herceptin
66	IDC	3	1+ (0)	1+ (0)	1+ (1.7)	10 cm (9.6)	+ (+)	Valproic Acid, FEC (5-FU, Epirubicin, Cyclophosphamide)
49	IDC	2	3+ (80)	1+ (0)	1+ (2.3)	4.3 cm (4.3)	- (-)	Paclitaxol, AC (Adriamycin / Doxorubicin and Cyclophosphamide)

OS, overall survival; CI, confidence interval; HR, hazard ratio; ER, estrogen receptor; PR, progesterone receptor, Her2, Human epidermal growth factor receptor 2; IDC, invasive ductal carcinoma; ILC- invasive lobular carcinoma; cm, centimeter

Table S8: Datasets used for retrospective gene expression survival analysis

Reference	GEO Accession Number	Availability	Sample Number	Platform Type
Anders et al., 2008 [S1]	GSE7849	Processed only	78	Affymetrix Human Genome U95 Version 2 Array
Bild et al., 2006 [S2]	GSE3143	Raw CEL files	158	Affymetrix Human Genome U95 Version 2 Array
Calabro et al., 2009 [S15]	GSE10510	Raw data avaiable	152	DKFZ Division of Molecular Genome Analysis Human Operon 4.0 oligo Array 35k
Chang et al., 2005 [S3]	NA	Processed only	295	Agilent
Chin et al., 2006 [S4]	NA	Processed only	118	Affymetrix U133AAofAv2
Chanrion et al., 2008 [S5]	GSE9893	Raw data avaiable	155	MLRG Human 21K V12.0
Desmedt et al., 2007 [S16]	GSE7390	Raw CEL files	198	Affymetrix U133A
Desmedt et al., 2009 [S6]	GSE16391	Raw CEL files	48	Affymetrix U133 Plus 2.0
Hu et al., 2006 [S7]	GSE1992	Processed only	99	Agilent
Ivshina et al., 2006 [S8]	GSE4922	Raw CEL files	249	Affymetrix U133A/B
Kok et al., 2009 [S17]	NA	Processed only	69	Agilent 44K oligo array
Loi et al., 2008 [S9]	GSE9195	Raw CEL files	77	Affymetrix U133 Plus 2.0
Loi et al., 2008 [S9]	GSE6532	Raw CEL files	414	Affymetrix U133A/B and plus2
Ma et al., 2004 [S10]	GSE1378, GSE 1379	Processed only	60	Custom 22K oligo array
Miller et al., 2005 [S11]	GSE3494	Raw CEL files	251	Affymetrix U133A/B
Pawitan et al., 2005 [S12]	GSE1456	Raw CEL files	159	Affymetrix U133A/B
Sabatier et al., 2010 [S18]	GSE21653	Raw CEL files	266	Affymetrix U133 Plus 2.0
Sabatier et al., 2010 [S18]	GSE17907	Raw CEL files	51	Affymetrix U133 Plus 2.0
Schmidt et al., 2008 [S13]	GSE11121	Raw CEL files	200	Affymetrix U133A
Wang et al., 2006 [14]	GSE2034	Raw CEL files	286	Affymetrix U133A
Zhang et al., 2008 [S19]	GSE12093	Raw CEL files	136	Affymetrix U133A
Expression Project for Oncology (expO) [S20]	GSE2109	Raw CEL files	353	Affymetrix U133 Plus 2.0

Citations correspond to references in the supplemental section

SUPPLEMENTAL REFERENCES

1. Carey LA, Perou CM, Livasy CA, et al. Race, breast cancer subtypes, and survival in the Carolina Breast Cancer Study. JAMA 2006;295:2492-502.
2. Tsai J, Lee JT, Wang W, et al. Discovery of a selective inhibitor of oncogenic B-Raf kinase with potent antimelanoma activity. Proc Natl Acad Sci U S A 2008;105:3041-6.
3. Louvet C, Szot GL, Lang J, et al. Tyrosine kinase inhibitors reverse type 1 diabetes in nonobese diabetic mice. Proc Natl Acad Sci U S A 2008;105:18895-900.
4. Artis DR, Bremer R, Gillette S, Hurt CR, Ibrahim PL, Zuckerman RL, inventors; Plexxikon, Inc., assignee. Molecular Scaffolds for Kinase Ligand Development. United States. 2005.
5. Junankar S, Eichten A, Kramer A, de Visser KE, Coussens LM. Analysis of immune cell infiltrates during squamous carcinoma development. J Invest Dermatology 2006;126 Suppl:36-43.
6. Irizarry RA, Bolstad BM, Collin F, Cope LM, Hobbs B, Speed TP. Summaries of Affymetrix GeneChip probe level data. Nucleic Acids Res 2003;31:e15.
7. Yang YH, Dudoit S, Luu P, Speed TP. Normalization for cDNA microarray data. In: Bittner M, Chen Y, Dorsel A, Dougherty E, editors. In Microarrays: Optical Technologies and Informatics: Proceedings of SPIE; 2001. p. 141–52.
8. Maglott D, Ostell J, Pruitt KD, Tatusova T. Entrez Gene: gene-centered information at NCBI. Nucleic Acids Res 2007;35:D26-31.